Published in final edited form as:
Nat Struct Mol Biol. 2018 January ; 25(1): 101–108. doi:10.1038/s41594-017-0005-5.

Histone octamer rearranges to adapt to DNA unwrapping

Silvija Bilokapic[1], **Mike Strauss**[2], and **Mario Halic**[1]

[1]Department of Biochemistry, Gene Center, LMU Munich, 81377 Munich, Germany

[2]Cryo EM Facility, Max Planck Institute of Biochemistry, 82152 Martinsried, Germany

Abstract

Nucleosomes, the basic unit of chromatin, package and regulate expression of eukaryotic genomes. Although the structure of the intact nucleosome has been studied, little is known about structures of its partially unwrapped, transient intermediates. In this study, we present 9 cryo EM structures of distinct conformations of nucleosome and subnucleosome particles. Our structures show that initial DNA breathing induces conformational changes in the histone octamer, particularly in histone H3, that propagate through the nucleosome and prevent symmetrical DNA opening. Rearrangements in the H2A–H2B dimer strengthen interaction with the unwrapping DNA and promote nucleosome stability. In agreement, cross-linked H2A–H2B that can not accommodate to the unwrapping of the DNA is not stably maintained in the nucleosome. H2A–H2B release and DNA unwrapping occur simultaneously indicating that DNA is essential in stabilizing the dimer in the nucleosome. Our structures reveal intrinsic nucleosomal plasticity that is required for nucleosome stability and might be exploited by extrinsic protein factors.

Keywords

nucleosome; chromatin; DNA unwrapping; transcription; cryo EM; nucleosome breathing; hexasome

Introduction

Packaging of DNA into chromatin regulates access to the genetic material, transcription, recombination and DNA repair. The fundamental repeating unit of the chromatin is the nucleosome1,2. The nucleosome core particle (NCP) is composed of two copies each of histones H2A, H2B, H3 and H4 around which is wrapped ~150bp of DNA3. DNA is stably packed on the histone surfaces by electrostatic interaction and hydrogen bonds between the DNA and the histone octamer3.

Corresponding author: Mario Halic : halic@genzentrum.lmu.de.

Author contributions. S.B. and M.H. designed the experiments. S.B. performed biochemical experiments and electron microscopy. M.S assisted with electron microscopy. S.B and M.H. analyzed the data. S.B. and M.H. wrote the paper.

Competing financial interests. The authors declare no competing financial interests.

Europe PMC Funders Author Manuscripts

Nucleosome structures are diverse due to histone variants, histone modifications and variations in their composition4. Recent studies show that nucleosomes are also highly dynamic and can adopt alternative conformations that are distinct from the canonical crystal structure. DNA wrapped around the histone octamer can transiently unwrap leading to DNA breathing, tightening, loosening, sliding and gaping5–8. It has been shown that under physiological conditions nucleosomal DNA unwraps and rewraps on a millisecond time scale5. This spontaneous unwrapping of nucleosomal DNA ends makes chromatin more accessible to DNA binding factors5,9,10.

Nucleosomes can also exhibit asymmetry with respect to histone content. The absence of one H2A–H2B dimer leads to the formation of the hexasome. The existence of open nucleosome particles and hexasomes was observed by ChIP-exo and MNase-seq experiments *in vivo*11. H2A–H2B dimer dissociation has also been observed during transcription, replication and remodeling12,13. It has been shown that the passage of the RNA Polymerase II through the nucleosome opens the nucleosome and generates the hexasome, which allows the nucleosome to remain partially assembled during transcription14,15. A collision of two nucleosomes during chromatin remodeling can also lead to nucleosome opening and hexasome formation16,17. *In vitro*, increased salt concentration facilitates nucleosome opening, showing that DNA breathing and hexasome formation is an intrinsic property of the nucleosome18,19. This might be facilitated by the activity of extrinsic protein factors such as transcription machinery, histone chaperones, ATP-dependent remodeling complexes and histone binding proteins1,2.

Although the structure of the intact nucleosome has been studied by crystallography, little is known about structures of the partially unwrapped, transient intermediates observed during transcription, DNA replication, and repair. Recent studies show that DNA unwraps from the stiffer side in an asymmetric way20,21. If the DNA flexibility were similar on two sides, DNA would stochastically unwrap from either side21, suggesting that the opening of one end helps to stabilize the other end. How the asymmetric unwrapping is achieved and what conformational changes occur in the nucleosome during DNA breathing is poorly understood. In this study, we used cryo EM to structurally characterize different states of nucleosome breathing and present 9 structures of distinct conformations of nucleosome and subnucleosome particles.

Results

Cryo EM structures of nucleosome breathing

We collected cryo EM data of nucleosome core particles (NCPs) assembled on a 601 DNA22 sequence that uniquely positions DNA on the histone octamer23 (Supplementary Fig. 1a). In dataset A, consisting of ~700 000 particles, NCPs can be clearly recognized in different orientations: as a disk, tilted views, and side views (Supplementary Fig. 1b, Table 1). In the 2D class averages, high-resolution details such as the DNA dyad, major and minor DNA grooves and histone α-helices can be seen (Supplementary Fig. 1c). We analyzed the data and solved the structure of NCP to 4.8 Å using all particles. Further classification of nucleosome core particles revealed several distinct classes of NCPs. The first class (Class 1) was reconstructed to 3.7 Å and has the appearance of a canonical nucleosome24–26 (Fig. 1a

and Supplementary Fig. 1d-g). Notably, we observed that ~10% of the particles occupied different states of DNA unwrapping (Fig. 1a). This is consistent with equilibrium measurements of the unwrapped state under physiological conditions5,20,27. These particles were classified into 3 distinct cryo EM maps and reconstructed to 5.4 Å (Class 2), 5.1 Å (Class 3) and 6.3 Å (Class 4) (Fig. 1a and Supplementary Fig. 2a-c).

We refined the X-ray model of the nucleosome assembled on 601 DNA28 and observed several changes in the structure of the nucleosome (Fig. 1b and Supplementary Fig. 3a-c). While the Class 1 cryo EM map and the X-ray structure are highly similar, in the Class 2 cryo EM map we observe an asymmetrical DNA bulge at one entry-exit site20,21 (Fig. 1a and Supplementary Fig. 2a). The DNA in the Class 2 structure is partially detached on one side of the nucleosome from the uH3 αN (uH3 for unwrapped side), that coordinates the last 13 base pairs (bp) of the DNA29. In this structure the entry-exit site DNA remains attached to the histone octamer by the weaker contacts with uH3 tail and the uH3 αN that slightly tilts towards the bulged DNA (Fig. 1a-c and Supplementary Fig. 3). The Class 2 structure shows that the H3 tail holds DNA when it detaches from the H3 αN, which is consistent with the data showing that nucleosomes missing the H3 tail are less stable30. The DNA bulging we observe in the Class 2 structure resembles the DNA bulging observed in the cryo EM map of Snf2 bound to the nucleosome31, indicating that this conformation is an inherent property of the nucleosome that is stabilized by the Snf2 chromatin remodeler.

In the Class 3 structure we observe further unwrapping of the DNA, which detached from the uH3 tail and uH3 αN (Fig. 1a-c and Supplementary Fig. 3). In this class ~15 bp of DNA are unwrapped from the histone octamer and the last contact with the DNA is formed by the H2A–H2B dimer (Fig. 1c). We also observe that the C-terminal region of uH2A, that binds entry-exit site DNA, is less defined on the side with unwrapped DNA in the Class 3 structure (Fig. 1b-c). This indicates that DNA is required to stabilize the H2A C-terminal region in the nucleosome.

DNA breathing induces conformational changes in the histone octamer

In the Class 4 structure, similar to Class 3, ~15bp of DNA are unwrapped and the H2A C-terminal region is delocalized. The unwrapped DNA is more flexible and visible only at low contour levels in this structure. The comparison of the Class 4 model with the Class 1-3 models also revealed global changes in the nucleosome structure. The nucleosome expands in the direction perpendicular to the symmetry axis with the distance between the superhelices2,3,29 SHL 2 and SHL -2 expanding from ~104 Å in Class 1-3 to ~106 Å in Class 4 (Supplementary Fig. 3d). Concomitantly, the nucleosome contracts along the symmetry axis in the Class 4 structure (Supplementary Fig. 3d).

In Class 2 and 3, beside changes near the unwrapped DNA, the overall structure of the histone octamer remains similar to the canonical nucleosome structure (Fig. 1c and Supplementary Fig. 1g, 3d). In Class 4, however, we observe major rearrangements of the histone octamer (Fig. 2a and Supplementary Fig. 4a, b). We calculated the root-mean-square deviation (RMSD) of the Class 1 and the Class 4 models to depict regions that exhibit the largest movements between these two maps. As expected, the RMSD data show that the histone octamer goes through major rearrangements near the unwrapped DNA. The uH3

αN, uH2A α2 and α3 and uH2B α1 and α2 that directly interact with the unwrapping DNA show large movements (Fig. 2a). Overall, the most pronounced changes in the histone octamer are found near the unwrapped DNA, the dyad, but also near the second DNA entry-exit site. The smallest changes in the histone octamer are found on the nucleosome half with the wrapped DNA where the second wH2A–H2B and wH4 show only minor movements (Fig. 2a and Supplementary Fig. 4b).

Rearrangement of H3–H4

In Class 4 we observe that uH3 αN helix is shorter and moves toward the unwrapping DNA (Fig. 2b). A shorter uH3 αN and the unwrapped DNA resemble the crystal structure of the CENP-A nucleosome32, indicating that the canonical nucleosome can adopt the same conformation and this conformation correlates with DNA unwrapping. In addition to a rearrangement of uH3 αN that directly interacts with the unwrapping DNA, we observe that uH3 α1 goes through a major rearrangement in the Class 4 structure (Fig. 2b). Our structures indicate that rearrangement of the uH3 αN, due to DNA unwrapping, leads to movement of the connecting uH3 α1 and α2 which bind the DNA at SHL -2 (Fig. 2a, b). This also pushes the DNA at SHL -2 outward (Fig. 2a, b). The uH3 α2 interacts at the dyad with the second wH3 α2, and a tilt of uH3 α2 leads to the inward tilt of wH3 α2 (Supplementary Fig. 4c). This pulls the DNA at the dyad toward the nucleosome center and results in the nucleosome contraction. Rearrangement of wH3 α2 leads to the movement of wH3 α1 on the wrapped half of the nucleosome which also pushes the DNA outward at SHL 2 (Fig. 2c). This also leads to the movement of the wH3 αN and the entry-exit site DNA on the wrapped half of the nucleosome towards the dyad, which might stabilize the interaction on that end (Fig. 2c). We also observe smaller rearrangement of uH4 α1 and α2 that bind the DNA at SHL -1 on the unwrapped half of the nucleosome (Supplementary Fig. 4d). Our data show that unwrapping of nucleosomal DNA rearranges uH3 αN and this alteration transmits to the opposite half of the nucleosome where wH3 αN and the entry-exit site DNA move closer together. One result of this change might a stabilization of the wH3 αN interaction with the DNA on the wrapped half of the nucleosome to prevent symmetrical DNA opening (Supplementary Fig. 4e).

Rearrangement of H2A–H2B

In the Class 2 structure the DNA at entry-exit site is bulged but still retained on the histone octamer by the H3 tail. In the Class 3 structure, the interaction between the H3 tail and the DNA is lost and the last contact between the histone octamer and the DNA is formed by the H2A–H2B (Fig. 3). The loop H2B L1, which connects the H2B helices α1 and α2, and the loop H2A L2, which connects H2A α2 and α3, make the last contact with the DNA at SHL 5.5 in the Class 3 structure (Fig. 3a, b). We observed that in the Class 3 structure DNA at SHL 5.5 moved outward which results in a weaker contact between the DNA and uH2A L2 and uH2B L1 (Fig. 3a, b). Weaker interaction with the DNA is also formed by the uH2B α1 at SHL 4.5 (Fig. 3a). Contacts of uH2A α1, uH2A L1 and uH2B L2 with the DNA at SHL 4.5 and SHL 3.5 remain stable in this structure (Fig. 3a). Our data show that in the Class 3 cryo EM map, DNA unwrapping reduces the interaction with the uH2A–H2B. In this class, uH2A–H2B remains in the same conformation as in the Class 1 structure (Fig. 3b).

In the Class 4 structure we observe rearrangement of the whole histone octamer which also strengthens interaction of uH2A–H2B with the DNA. The DNA at SHL 5.5 in the Class 4 structure is in a similar position as in the Class 3 structure. In the Class 4 structure, however, the uH2A α2 and α3 (H2A L2) and uH2B α1 and α2 (H2B L1) are tilted and moved towards the unwrapping DNA at SHL 5.5 (Fig. 3c, d). The loops H2B L1 and H2A L2 make the last contact with the DNA in the Class 4 structure and the tilt of their α-helices strengthens the contact with the unwrapping DNA (Fig. 3c). This interaction is visible at high contour levels and is comparable to other histone-DNA interactions in the Class 4 structure (Fig. 3c). H2B α3 and αC and H2A α3 did not change their conformation (Fig. 3d), which indicates that H2A–H2B goes through internal rearrangement as DNA unwraps. This internal rearrangement of H2A–H2B to accommodate to DNA unwrapping might prevent further DNA unwrapping and stabilize the nucleosome.

Plasticity of H2A–H2B is required for nucleosome stability

The observed plasticity of H2A–H2B dimer might be crucial for nucleosome stability. To determine if adjustment of H2A–H2B to DNA movements is required for DNA binding and nucleosome stability, we assembled the nucleosome with the cross-linked dimers (Supplementary Fig. 5a, b). The cross-linked H2A–H2B is fully functional in its interaction with the H3–H4 tetramer and the complex can be purified on size exclusion chromatography (Supplementary Fig. 5a, b). When we assembled the nucleosome with the cross-linked H2A–H2B dimers, we obtained mainly hexasomes containing one cross-linked H2A–H2B and only a very low quantity of nucleosomes as visible on a native gel (Fig. 4a). To enforce nucleosome formation we have added native and cross-linked H2A–H2B to the assembled hexasome (Fig. 4b). The native H2A–H2B was efficiently incorporated into the hexasome forming the nucleosome containing one cross-linked and one native H2A–H2B. Cross-linked H2A–H2B, however, was not stably incorporated into the hexasome (Fig. 4b), indicating that H2A–H2B plasticity is required for nucleosome stability.

To determine if plasticity of a globular domain of H2A–H2B is required for the nucleosome stability, we added native and cross-linked globular H2A–H2B dimers to the hexasome. While globular native H2A–H2B was assembled into the nucleosome, cross-linked globular H2A–H2B was not stably bound (Fig. 4c). Consistent with our structures, these data show that plasticity of the globular domain of H2A–H2B is required for the stability of the nucleosome.

To test if histone chaperones might be able to incorporate cross-linked H2A–H2B, we used Nap1 in the nucleosome assembly reaction. When full length or globular H2A–H2B were cross-linked, the Nap1 chaperone also assembled the hexasome (Fig. 4d). In agreement with our previous assays (Fig. 4b), Nap1 was able to incorporate native, but not cross-linked H2A–H2B into the hexasome containing one cross-linked H2A–H2B (Fig. 4d-e and Supplementary Fig. 5c-e). H2A–H2B cross-linking did not affect its interaction with Nap1 further supporting that cross-linked H2A–H2B is fully functional in its interactions (Supplementary Fig. 5c, d). These data show that chaperone mediated assembly of nucleosome also requires plasticity of the H2A–H2B globular domain.

Our data show that cross-linked H2A–H2B can be assembled into the hexasome, but it is not stably bound to the nucleosome. This indicates that incorporation and stability of the first and the second H2A–H2B in the nucleosome has different requirements. Incorporation of the first dimer into hexasome can tolerate dimer rigidity, however, the stability of the second dimer in the nucleosome requires some degree of plasticity of the H2A–H2B globular domain (Fig. 4f).

H2A–H2B dissociation and hexamer formation

In the second dataset (B) we observed many atypical particles with DNA protruding from the nucleosome core particle in 2D class averages (Supplementary Fig. 6a-e, Table 2). This indicated that the DNA partially detached from the histone octamer. We classified these images and obtained multiple structures of distinct nucleosome intermediates and subnucleosome particles with differently organized DNA (Fig. 5a-e and Supplementary Fig. 7). In these structures the DNA is more flexible and is not well resolved. The DNA flexibility also limits the quality of alignment and resolution of these intermediates. Importantly, the organization of the histone core is sufficiently well resolved to unambiguously dock crystal structures, and compare the maps. The overall resolution of these maps ranges from 8 to 11 Å (Supplementary Fig. 7) with histones being better resolved than DNA (Supplementary Fig. 8).

In Class 5, we observe further DNA unwrapping from the histone core (Fig. 5a). The contact of DNA with the loops uH2A L2 and uH2B L1 is now lost. This leads to unwrapping of ~25 bp of DNA from the histone octamer and only ~120 bp are organized by the nucleosome (Fig. 5a and Supplementary Fig. 8a). In this class, the last contact with the DNA is made by uH2B α1, with the DNA protruding from the histone octamer after the contact (Fig. 5a). The uH2A–H2B dimer shows higher flexibility on the side with unwrapped DNA (Supplementary Fig. 8a). In the next structure (Class 6) contact between DNA and uH2B α1 is lost and an additional ~5 bp of DNA unwrap from the histone octamer (Fig. 5b and Supplementary Fig. 8b). This leads to further destabilization of uH2A–H2B that is now less defined compared to other histones (Supplementary Fig. 8b).

In the next step of DNA unwrapping (Class 7), the DNA contact with H2A α1 is lost and ~35 bp of DNA are not organized by the histone octamer (Fig. 5c and Supplementary Fig. 8c). In Class 7, uH2A–H2B interacts with the DNA only with the uH2A L1 and uH2B L2 loops, which is not sufficient to stably maintain uH2A–H2B in the nucleosome (Fig. 5c). In this structure we observed only a partial and weak density for the uH2A–H2B dimer indicating high flexibility (Fig. 5c and Supplementary Fig. 8c). This is consistent with the finding that H2A–H2B shows an increased distance from the dyad before its dissociation19. Our data show that DNA is required to stabilize H2A–H2B in the nucleosome.

In classes 8 and 9, the density for the H2A–H2B dimer is very weak or missing indicating H2A–H2B dissociation and formation of the hexasome (Fig. 5d, e). The remaining histones in the hexasome are globally organized similar to the canonical nucleosome structure, consistent with SAX data and a recent crystal structure17,33. In the absence of one H2A–H2B histone dimer the DNA further unwraps leaving only ~110 nucleotides organized by the histone hexamer (Fig. 5d, e and Supplementary Fig. 8d-e). In the hexasome structures,

the H4 loop L2 that connects H4 helices α2 and α3 makes the last contact with the DNA at SHL 2.5. We found two alternative conformations of the hexasome. In Class 8, the unbound DNA continues its path in a tangential direction after the last contact with the histone H4 loop L2 (Fig. 5d and Supplementary Fig. 8d). In Class 9, the DNA moved and protrudes from both sides of the hexasome (Fig. 5e and Supplementary Fig. 8e). In this class ~15 bp of DNA protrude from the hexasome after the last contact with the H4 loop L2. Approximately 25 bp of DNA protrude from the entry-exit site on the opposite side of the hexasome (Fig. 5e). These data show that reduced contacts of histones with the DNA in the hexasome lead to increased DNA sliding, which is consistent with biochemical observations34. This property of the hexasome might be used by external factors to gain access to DNA or to move the nucleosome and may play an important role in transcription, replication, and chromatin remodeling.

Discussion

Studies of the intrinsic properties and dynamics of the nucleosome are critical for understanding how various nuclear machineries gain access to DNA *in vivo*. In this work, we captured multiple steps of DNA unwrapping from the histone octamer by cryo EM, consistent with nucleosome states observed by single molecule experiments5,9,19,20,35. We found that DNA unwrapping induces conformational changes in the histone octamer that are necessary to stabilize the nucleosome.

Previous studies have reported that DNA unwraps from the nucleosome in an asymmetrical way20,21. If the DNA flexibility were similar on both sides, DNA would unwrap stochastically from either side21. These studies suggest that the opening of one end helps to stabilize the other end. In our structures we observe rearrangements of histones not only near the site of DNA unwrapping, but in the entire histone octamer. Specifically we observe that DNA unwrapping rearranges H3 on the unwrapped half of the nucleosome and this propagates to the second H3 and to the entry-exit DNA on the other end. H3 αN and the DNA on the wrapped half of the nucleosome move closer and toward the dyad which might stabilize the DNA on that side. Our structures reveal changes in the histone octamer that can explain why nucleosomes open asymmetrically, even on symmetrical DNA.

Our structural and biochemical data reveal that plasticity of H2A–H2B is required for nucleosome stability. We observe that several α-helices of H2A–H2B tilt toward the unwrapping DNA to maintain the interaction. Additionally, cross-linked H2A–H2B that cannot accommodate to DNA unwrapping is not stably maintained in the nucleosome. This indicates that the observed internal plasticity of H2A–H2B is essential for nucleosome stability. Our data suggest that H2A–H2B plasticity prevents further DNA unwrapping and promotes DNA re-wrapping. This is consistent with single molecule data showing that ~10% of nucleosomes have entry-exit site DNA unwrapped under physiological conditions and that DNA unwraps and re-wraps on a millisecond time scale9,20.

We observe that DNA unwrapping and H2A–H2B release occur together and that DNA is required to stabilize the H2A–H2B dimer in the nucleosome. These data suggest that if an extrinsic factor prevents DNA re-wrapping, this will destabilize H2A–H2B and facilitate

further DNA unwrapping and nucleosome opening beyond the first 15 bp. In agreement, binding of an extrinsic protein to nucleosomes drives the conformational equilibrium toward the unwrapped DNA state9. Moreover, RNA polymerase II has been shown to use intrinsic nucleosomal fluctuations to transcribe around the nucleosome, rather than actively separating DNA from histones10. Our structures provide a mechanistic explanation of intrinsic nucleosomal dynamics that are utilized by RNA polymerase II and other DNA-based enzymes.

Methods

Nucleosome reconstitution

Xenopus laevis histones were co-expressed and co-purified as soluble H2A–H2B histone dimers and (H3–H4)2 histone tetramers, as described23,36,37. The globular H2A and H2B were expressed as inclusion bodies and purified under denaturing conditions as described38. The refolded histone pair was further purified using ion exchange and size exclusion chromatography. Cross-linked H2A–H2B, after quenching the cross-linking reaction, were desalted on the PD10 desalting column (15 mM HEPES-NaOH pH 7.5, 2 mM NaCl, 1 mM DTT) and concentrated. The purified histone pairs were used to assemble histone octamer in 25 mM HEPES-NaOH pH 7.5, 2 mM NaCl, 1 mM DTT. To obtain the histone octamer, a 2.8-fold excess of wild type or cross-linked H2A–H2B histone dimer was mixed with H3–H4 histone tetramer and subsequently purified by size exclusion chromatography equilibrated in 15 mM HEPES-NaOH pH 7.5, 2 mM NaCl, 1 mM DTT (Supplementary Fig. 5a-b). DNA for nucleosome reconstitution was PCR amplified from a plasmid containing the 601 DNA sequence. The PCR product was purified by phenol-chloroform extraction. After ethanol precipitation, the DNA was re-suspended in 25 mM HEPES-NaOH pH 7.5, 2 M NaCl, 1 mM DTT.

After size exclusion chromatography, the histone octamer peak fractions were mixed with DNA and placed into a dialysis button made from the lid of an Eppendorf tube. The nucleosome reconstitution was done by 'double bag' dialysis23,37. The dialysis buttons, containing 0.25ml of the histone octamer:DNA mixture, were placed inside a dialysis bag, filled with ~50 ml of size exclusion buffer. The dialysis bag was immersed into a 1l of buffer containing 15 mM HEPES-NaOH pH 7.5, 1M NaCl, 1 mM DTT and dialysed over-night at +4 °C. The next day the dialysis bag was immersed into a 1l low salt buffer. The dialysis into low salt buffer was done for 5-6 hours. Finally, in the last step only the dialysis buttons were dialysed for 1-2 hours in the low salt buffer. NCP for dataset 1 were dialysed to final concentration of 50 mM NaCl, 15 mM HEPES-NaOH pH 7.5, 1mM DTT. For the dataset 2, the NCPs were dialysed to 250 mM NaCl, 15 mM HEPES-NaOH pH 7.5, 1mM DTT. The samples were concentrated to 2 mg/ml for cryoEM grids preparation. The reconstitution results were analysed on 6% native PAGE.

Nap1:H2A–H2B complex formation

1.5 μg of each histone dimer (wild-type and cross-linked sample) were mixed with 4 μg Nap1 chaperone in 30 mM HEPES pH 7.5, 200 mM NaCl and 1 mM DTT to a final volume of 20 μl. The samples were incubated for 60 min at room temperature. Upon the addition of

the glycerol, to a final concetration of 4% v/v, the samples were loaded on 6% native polyacrylamide gel. The gel was run in 1x TBE at 120V for 120 min in the cold room at 4ºC.

H2A–H2B histone dimer cross-linking

H2A–H2B histone dimer was diluted to 0.5 mg/ml with 30 mM HEPES pH 7.5, 2 M NaCl and 1 mM DTT. The glutaraldehyde was added to a final concentration of 0.005% (v/v) and the sample was incubated for 5 min at the room temperature. The cross-linking was quenched with 50mM Tris/HCl pH 7.5 (final concentration). For the globular H2A–H2B dimer, the glutaraldehyde concentration was increased to 0.01%.

Nucleosome formation using hexasome and H2A–H2B dimer

The hexasome was obtained during the nucleosome assembly with the cross-linked H2A–H2B. 2.3 pmol hexasome were incubated with increasing amounts of the wild-type and cross-linked H2A–H2B histone dimer (3.5, 7 and 14 pmol of histone dimer). We used full-length and globular H2A–H2B dimer. The reaction was incubated at 30 °C for 1 hour in 15 mM HEPES-NaOH pH 7.5, 100mM NaCl, 1mM DTT and analysed on 6% native PAGE.

Nucleosome reconstitution using Nap1 chaperone

H3-H4 histone tetramer was mixed with an access of crosslinked H2A-H2B dimer and purified by size exclusion chromatography. 15 pmol of histone protein core were mixed with 80 pmol Nap1 chaperone in the buffer with the final composition 10 mM HEPES pH 7.5, 50mM KCl, 5mM MgCl2, 0.5mM EGTA, 0.1 mM EDTA, 0.1mg/ml BSA, 5% glycerol. The mixture was supplemented with an additional wild-type or cross-linked H2A–H2B dimer (7, 14 and 28 pmol). DNA, dissolved in water, was added at the end. A 20 µl reaction was incubated at 30 °C for 4 hours and 10 µl was loaded on 6% native PAGE.

CryoEM grid preparation and data collection

Quantifoil R2/1 and R1.2/1.3 holey carbon grids were used. A Leica EM GP automatic plunge freezer was used for the sample vitrification. Temperature in the chamber was kept at +15 °C and the humidity at 95%. 3µl of NCP sample were applied to freshly glow-discharged grid. After a 3 s blotting time, grids were plunge-frozen in the liquid ethane. For the dataset A, electron micrographs were recorded on a FEI Titan Halo (FEI) at 300 kV with a Falcon 2 direct electron detector (FEI) (~2000 micrographs) (MPI of Biochemistry, Martinsried, Germany) and FEI Titan Krios at 300 kV with a Gatan Summit K2 electron detector (~750 micrographs) (Necen, Leiden, Netherlands). For the data collected on the Titan Halo the nominal magnification was 75 000 x resulting in an image pixel size of 1.4 Å per pixel on the object scale. Data were collected in a defocus range of 10 000 Å – 40 000 Å with a total exposure of 100 e/Å^2. 40 frames were collected and aligned with the Unblur software package using a dose filter39. For the data collected on Titan Krios image pixel size was 1.36 Å per pixel on the object scale. Data were collected in a defocus range of 10 000 Å – 40 000 Å with a total exposure of 80 e/Å^2. 60 frames were collected and aligned with the Unblur software package using a dose filter. For the second dataset B we collected ~1000 micrographs on FEI Titan Halo as described above.

Several thousand particles were manually picked and carefully cleaned in XMIPP40 to remove inconsistent particles. The resulting useful particles were then used for semi-automatic and automatic particle picking in XMIPP. The contrast transfer function parameters were determined using CTFFIND441. The 2D class averages were generated with Relion software package42. Inconsistent class averages were removed from further data analysis. The 3D refinements and classifications were subsequently done in Relion. All final refinements were done in Relion using the auto refine option. The initial reference was filtered to 60 Å in Relion. C1 symmetry was applied during refinements for all classes with exception of Class 1 which was refined with C2 symmetry. NCP particles collected on Titan Halo (Falcon 2) refined to 3.9 Å, while NCP particles collected on Titan Krios (K2) refined to 3.7 Å. Class 1 structure contains only data collected on Titan Krios, since merging 2 datasets resulted in a reconstruction with slightly lower resolution due to necessary interpolation. Classes 2-4 contain data collected on Titan Krios and Titan Halo. Lower particle number in these classes was a limiting factor and mixing two datasets resulted in improved structures. Particles were split into 2 datasets and refined independently and the resolution was determined using the 0.143 cut-off (Relion auto refine option). Local resolution was determined with Relion 2.0. All maps were filtered to local resolution using Relion 2.0 with a B-factor determined by Relion.

FSCwork and FSCfree show no over-fitting during the refinement (Supplementary Fig. 1e and 2b). To generate FSCwork and FSCfree, atoms from the models built with the combined maps were randomly displaced to 0.5 Å, and then subjected to refinement against one (‘work’) of two half maps obtained from independent half data sets. An FSC curve (FSCwork) was calculated between the refined model and the half map used for refinement. As cross-validation, a second FSC curve (FSCfree) was calculated between the refined model and the other half map (‘free’) not used in refinement.

Molecular models were built using Coot43 and refined in Phenix44. The Chimera software package was used for rigid body fitting of models45. Molecular models for classes 1-4 were superimposed in Chimera using matchmaker option. To determine the accuracy of the model and uncertainty in the refinement of the model, independent models for two half data sets were analyzed. To show uncertainty, model variation was calculated in Chimera as RMSD of Cα backbone between two models (half1 and half2 model) (Supplementary Fig. 9a). These data show that for Class 1 uncertainty is less than 0.2 Å for most of the model. For Class 4 uncertainty is as expected higher, but lower than 1.0 Å for most regions. Additionally, to depict changes we have superimposed the Class 4 cryo EM map with the Class 1 model and Class 1 map (Supplementary Fig. 9b). We have also calculated the difference map between Class 4 and Class 1 map (filtered to 6 Å) (Supplementary Fig. 9b). These data show clear differences between Class 1 and Class 4 maps at H2A–H2B near SHL 5 and in H3.

For Classes 5-9, PDB 3LZ1 was docked using the Chimera software package45. NCP DNA that was not visible in the structure was removed and replaced by a straight DNA helix in Chimera. Visualization of all cryo-EM maps was done with Chimera.

Data availability

EM densities have been deposited in the Electron Microscopy Data Bank under accession codes EMD-3947 (Class 1), EMD-3948 (Class 2), EMD-3949 (Class 3), EMD-3950 (Class 4), EMD-3931 (Class 5), EMD-3930 (Class 6), EMD-3929 (Class 7), EMD-3926 (Class 8), EMD-3925 (Class 9). The coordinates of EM-based models have been deposited in the Protein Data Bank under accession codes PDB 6ESF (Class 1), 6ESG (Class 2), 6ESH (Class 3), 6ESI (Class 4). All other data are available from the corresponding author upon reasonable request.. A Life Sciences Reporting Summary for this article is available.

Supplementary Material

Refer to Web version on PubMed Central for supplementary material.

Acknowledgments

We would like to thank E. Conti and the Cryo EM facility at Max Planck Institute for Biochemistry in Martinsried for access to cryo EM microscopes. Without their support this work would not be possible. We also acknowledge Instruct for supporting the data collection at NECEN in Leiden. The authors would like to thank R. Büchner and H. Thomas for the help with the histone purification and S. Jaklin for excellent technical assistance. We also thank the Halic lab for comments on the manuscript. This work was supported by the ERC-smallRNAhet-309584 and the Instruct PID 1498.

References

1. Cutter AR, Hayes JJ. A brief review of nucleosome structure. FEBS Lett. 2015; 589:2914–2922. [PubMed: 25980611]
2. Andrews AJ, Luger K. Nucleosome structure(s) and stability: variations on a theme. Annu Rev Biophys. 2011; 40:99–117. [PubMed: 21332355]
3. Luger K, Mäder AW, Richmond RK, Sargent DF, Richmond TJ. Crystal structure of the nucleosome core particle at 2.8 A resolution. Nature. 1997; 389:251–260. [PubMed: 9305837]
4. Luger K, Dechassa ML, Tremethick DJ. New insights into nucleosome and chromatin structure: an ordered state or a disordered affair? Nat Rev Mol Cell Biol. 2012; 13:436–447. [PubMed: 22722606]
5. Li G, Levitus M, Bustamante C, Widom J. Rapid spontaneous accessibility of nucleosomal DNA. Nat Struct Mol Biol. 2005; 12:46–53. [PubMed: 15580276]
6. Miyagi A, Ando T, Lyubchenko YL. Dynamics of nucleosomes assessed with time-lapse high-speed atomic force microscopy. Biochemistry. 2011; 50:7901–7908. [PubMed: 21846149]
7. Lyubchenko YL. Nanoscale Nucleosome Dynamics Assessed with Time-lapse AFM. Biophys Rev. 2014; 6:181–190. [PubMed: 24839467]
8. Ngo TTM, Ha T. Nucleosomes undergo slow spontaneous gaping. Nucleic Acids Res. 2015; 43:3964–3971. [PubMed: 25824950]
9. Li G, Widom J. Nucleosomes facilitate their own invasion. Nat Struct Mol Biol. 2004; 11:763–769. [PubMed: 15258568]
10. Hodges C, Bintu L, Lubkowska L, Kashlev M, Bustamante C. Nucleosomal fluctuations govern the transcription dynamics of RNA polymerase II. Science. 2009; 325:626–628. [PubMed: 19644123]
11. Rhee HS, Bataille AR, Zhang L, Pugh BF. Subnucleosomal structures and nucleosome asymmetry across a genome. Cell. 2014; 159:1377–1388. [PubMed: 25480300]
12. Sheinin MY, Li M, Soltani M, Luger K, Wang MD. Torque modulates nucleosome stability and facilitates H2A–H2B dimer loss. Nat Commun. 2013; 4:2579. [PubMed: 24113677]
13. Bintu L, et al. The elongation rate of RNA polymerase determines the fate of transcribed nucleosomes. Nat Struct Mol Biol. 2011; 18:1394–1399. [PubMed: 22081017]

14. Bintu L, et al. The elongation rate of RNA polymerase determines the fate of transcribed nucleosomes. Nat Struct Mol Biol. 2011; 18:1394–1399. [PubMed: 22081017]
15. Kireeva ML, et al. Nucleosome remodeling induced by RNA polymerase II: loss of the H2A–H2B dimer during transcription. Mol Cell. 2002; 9:541–552. [PubMed: 11931762]
16. Engeholm M, et al. Nucleosomes can invade DNA territories occupied by their neighbors. Nat Struct Mol Biol. 2009; 16:151–158. [PubMed: 19182801]
17. Kato D, et al. Crystal structure of the overlapping dinucleosome composed of hexasome and octasome. Science. 2017; 356:205–208. [PubMed: 28408607]
18. Kireeva ML, et al. Nucleosome remodeling induced by RNA polymerase II: loss of the H2A–H2B dimer during transcription. Mol Cell. 2002; 9:541–552. [PubMed: 11931762]
19. Böhm V, et al. Nucleosome accessibility governed by the dimer/tetramer interface. Nucleic Acids Res. 2011; 39:3093–3102. [PubMed: 21177647]
20. Chen Y, et al. Asymmetric unwrapping of nucleosomal DNA propagates asymmetric opening and dissociation of the histone core. Proc Natl Acad Sci USA. 2017; 114:334–339. [PubMed: 28028239]
21. Ngo TTM, Zhang Q, Zhou R, Yodh JG, Ha T. Asymmetric unwrapping of nucleosomes under tension directed by DNA local flexibility. Cell. 2015; 160:1135–1144. [PubMed: 25768909]
22. Lowary PT, Widom J. New DNA sequence rules for high affinity binding to histone octamer and sequence-directed nucleosome positioning. J Mol Biol. 1998; 276:19–42. [PubMed: 9514715]
23. Ivic N, Groschup B, Bilokapic S, Halic M. Simplified Method for Rapid Purification of Soluble Histones. Croatica chemica acta. 2016; 89:153–162.
24. Zocco M, Marasovic M, Pisacane P, Bilokapic S, Halic M. The Chp1 chromodomain binds the H3K9me tail and the nucleosome core to assemble heterochromatin. Cell Discov. 2016; 2:16004. [PubMed: 27462451]
25. Luger K, Mäder AW, Richmond RK, Sargent DF, Richmond TJ. Crystal structure of the nucleosome core particle at 2.8 A resolution. Nature. 1997; 389:251–260. [PubMed: 9305837]
26. Chua EYD, et al. 3.9 Å structure of the nucleosome core particle determined by phase-plate cryo-EM. Nucleic Acids Res. 2016; 44:8013–8019. [PubMed: 27563056]
27. Chen Y, et al. Revealing transient structures of nucleosomes as DNA unwinds. Nucleic Acids Res. 2014; 42:8767–8776. [PubMed: 24990379]
28. Vasudevan D, Chua EYD, Davey CA. Crystal structures of nucleosome core particles containing the '601' strong positioning sequence. J Mol Biol. 2010; 403:1–10. [PubMed: 20800598]
29. McGinty RK, Tan S. Nucleosome structure and function. Chem Rev. 2015; 115:2255–2273. [PubMed: 25495456]
30. Iwasaki W, et al. Contribution of histone N-terminal tails to the structure and stability of nucleosomes. FEBS Open Bio. 2013; 3:363–369.
31. Liu X, Li M, Xia X, Li X, Chen Z. Mechanism of chromatin remodelling revealed by the Snf2-nucleosome structure. Nature. 2017; 544:440–445. [PubMed: 28424519]
32. Tachiwana H, et al. Crystal structure of the human centromeric nucleosome containing CENP-A. Nature. 2011; 476:232–235. [PubMed: 21743476]
33. Arimura Y, Tachiwana H, Oda T, Sato M, Kurumizaka H. Structural analysis of the hexasome, lacking one histone H2A–H2B dimer from the conventional nucleosome. Biochemistry. 2012; 51:3302–3309. [PubMed: 22448809]
34. Park Y-J, Chodaparambil JV, Bao Y, McBryant SJ, Luger K. Nucleosome assembly protein 1 exchanges histone H2A–H2B dimers and assists nucleosome sliding. J Biol Chem. 2005; 280:1817–1825. [PubMed: 15516689]
35. Hall MA, et al. High-resolution dynamic mapping of histone-DNA interactions in a nucleosome. Nat Struct Mol Biol. 2009; 16:124–129. [PubMed: 19136959]
36. Anderson M, et al. Co-expression as a convenient method for the production and purification of core histones in bacteria. Protein Expr Purif. 2010; 72:194–204. [PubMed: 20347990]
37. Shim Y, Duan M-R, Chen X, Smerdon MJ, Min J-H. Polycistronic coexpression and nondenaturing purification of histone octamers. Anal Biochem. 2012; 427:190–192. [PubMed: 22617796]

38. Luger K, Rechsteiner TJ, Richmond TJ. Expression and purification of recombinant histones and nucleosome reconstitution. Methods Mol Biol. 1999; 119:1–16. [PubMed: 10804500]

39. Grant T, Grigorieff N. Measuring the optimal exposure for single particle cryo-EM using a 2.6 Å reconstruction of rotavirus VP6. Elife. 2015; 4:e06980. [PubMed: 26023829]

40. Scheres SHW, Núñez-Ramírez R, Sorzano COS, Carazo JM, Marabini R. Image processing for electron microscopy single-particle analysis using XMIPP. Nat Protoc. 2008; 3:977–990. [PubMed: 18536645]

41. Rohou A, Grigorieff N. CTFFIND4: Fast and accurate defocus estimation from electron micrographs. J Struct Biol. 2015; 192:216–221. [PubMed: 26278980]

42. Scheres SHW. RELION: implementation of a Bayesian approach to cryo-EM structure determination. J Struct Biol. 2012; 180:519–530. [PubMed: 23000701]

43. Emsley P, Lohkamp B, Scott WG, Cowtan K. Features and development of Coot. Acta Crystallogr D Biol Crystallogr. 2010; 66:486–501. [PubMed: 20383002]

44. Adams PD, et al. PHENIX: a comprehensive Python-based system for macromolecular structure solution. Acta Crystallogr D Biol Crystallogr. 2010; 66:213–221. [PubMed: 20124702]

45. Pettersen EF, et al. UCSF Chimera--a visualization system for exploratory research and analysis. J Comput Chem. 2004; 25:1605–1612. [PubMed: 15264254]

Europe PMC Funders Author Manuscripts

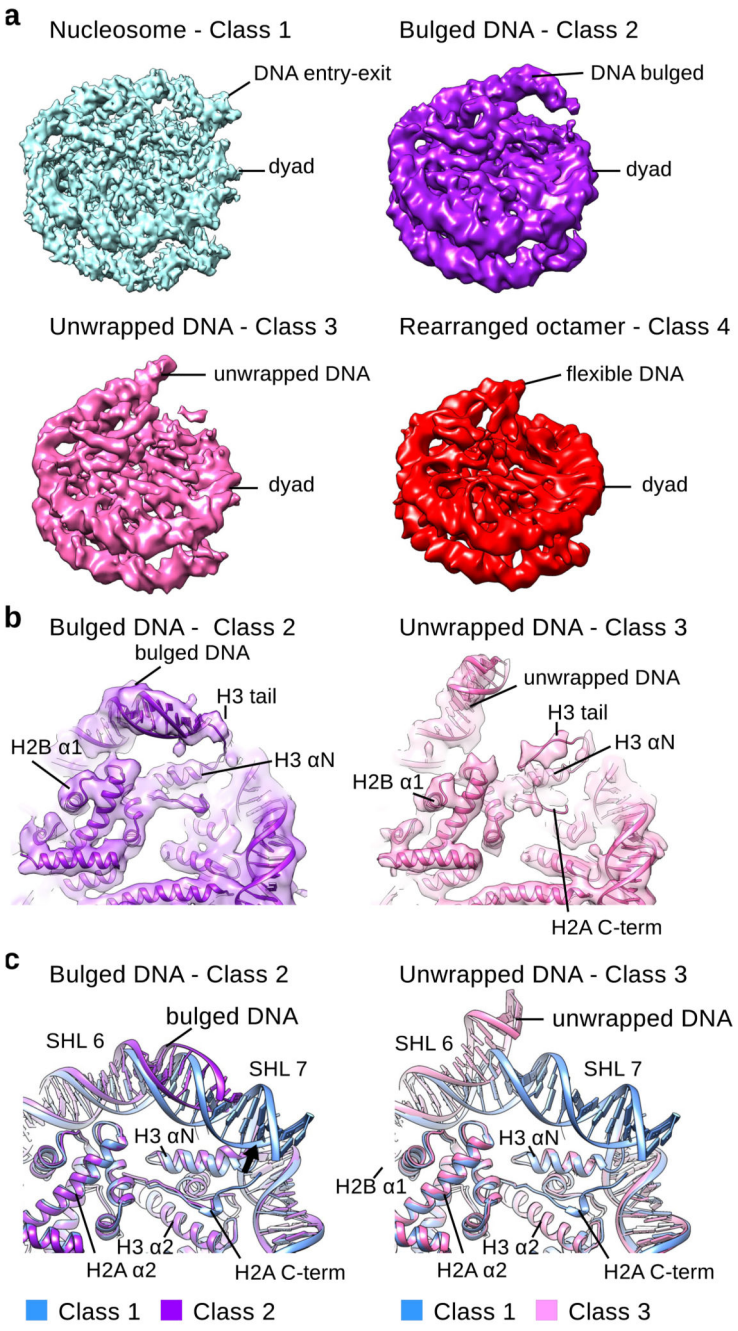

Fig. 1. Cryo-EM reconstructions of NCP with unwrapped DNA.

a, Cryo-EM maps of the canonical NCP (Class 1) and NCPs with unwrapped DNA (Class 2-4). ~10 % of particles have unwrapped DNA at one entry-exit site. The Class 1 map (blue) was reconstructed to 3.7 Å (0.143 cutoff in FSC curve); the Class 2 map (purple) was reconstructed to 5.4 Å; the Class 3 map (pink) was reconstructed to 5.1 Å; the Class 4 map (red) was reconstructed to 6.3 Å. All maps are shown at similar contour levels.

b, Fitting of the Class 2 (purple) and the Class 3 (pink) models into cryo EM maps. The X-ray structure of the NCP (PDB:3LZ1) was refined into the Class 2 and Class 3 cryo EM

maps. In the Class 2 map the H3 tail binds the DNA and retains it at the histone octamer. In the Class 3 map, DNA is detached from the H3 tail. H2A C-terminal region is delocalized in the Class 3 structure.

c, Comparison of the Class 1 model of NCP (blue) with Class 2 (purple) and Class 3 (pink) models. In the Class 2 structure DNA bulges but remains attached to the octamer. In the Class 3 structure entry-exit site DNA detaches from the octamer. This leads to delocalization of H2A C-terminal tail which binds the entry-exit site DNA. Other histones are in the canonical conformation.

Europe PMC Funders Author Manuscripts

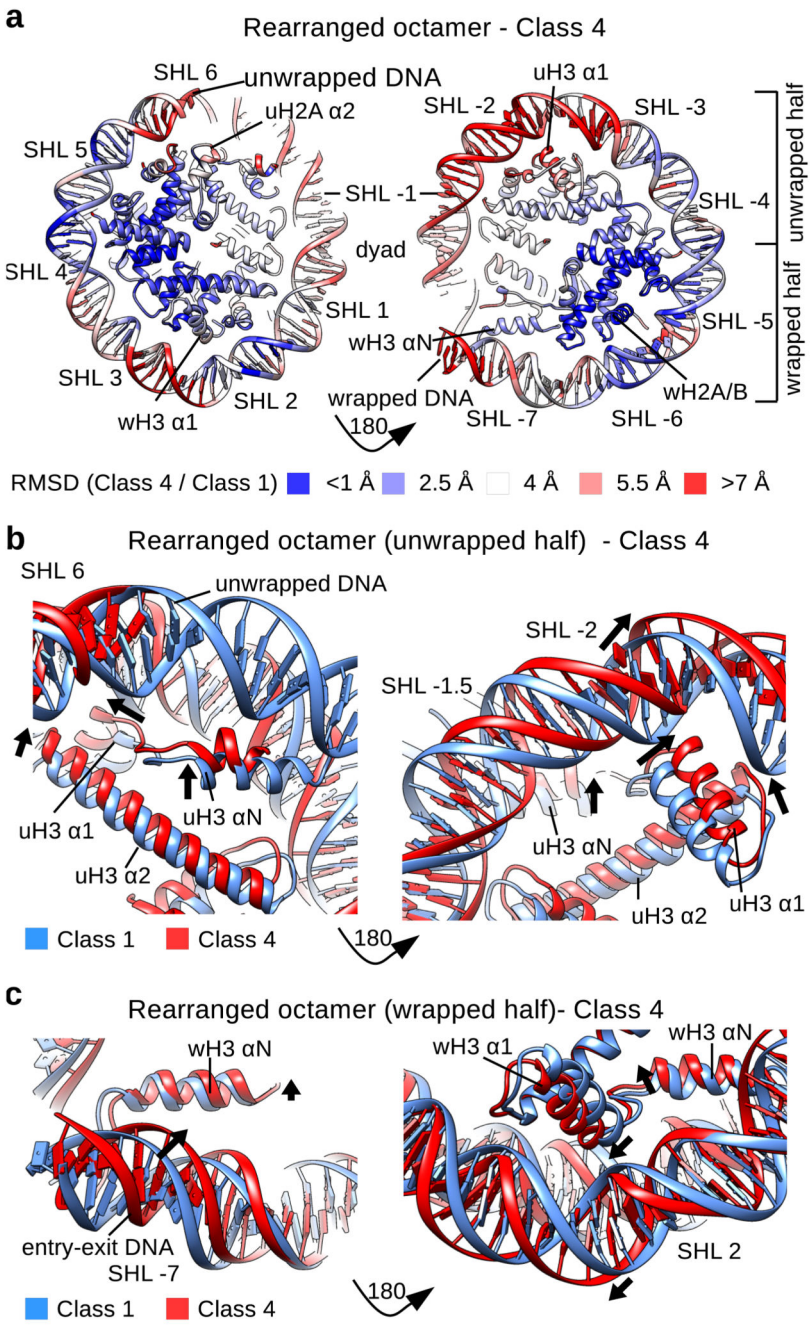

Fig. 2. Histone octamer rearranges when DNA unwraps.

a, RMSD (Cα) between the models for the Class 1 and the Class 4 structures showing the extent of rearrangements in the NCP. The DNA at SHL +- 2 and SHL +- 6-7 shows the largets movements between the Class 4 and canonical nucleosome structures. H3 αN, H3 α1 and α2, uH2A α2 and uH2B α1 show the largest rearrangements in the histone octamer.

b, Conformational rearrangement of H3 in the half of the nucleosome with the unwrapped DNA. uH3 αN, uH3 α1 and uH3 α2 move in the Class 4 structure when compared to the Class 1 structure. DNA at SHL -2 moves outward.

c, Conformational rearrangement of H3 in the half of the nucleosome with the wrapped DNA. wH3 αN and wH3 α1 move in the Class 4 structure when compared to the Class 1 structure. DNA at SHL 2 moves outward. wH3 αN and DNA at SHL -7 (second entry-exit site) move inward.

Europe PMC Funders Author Manuscripts

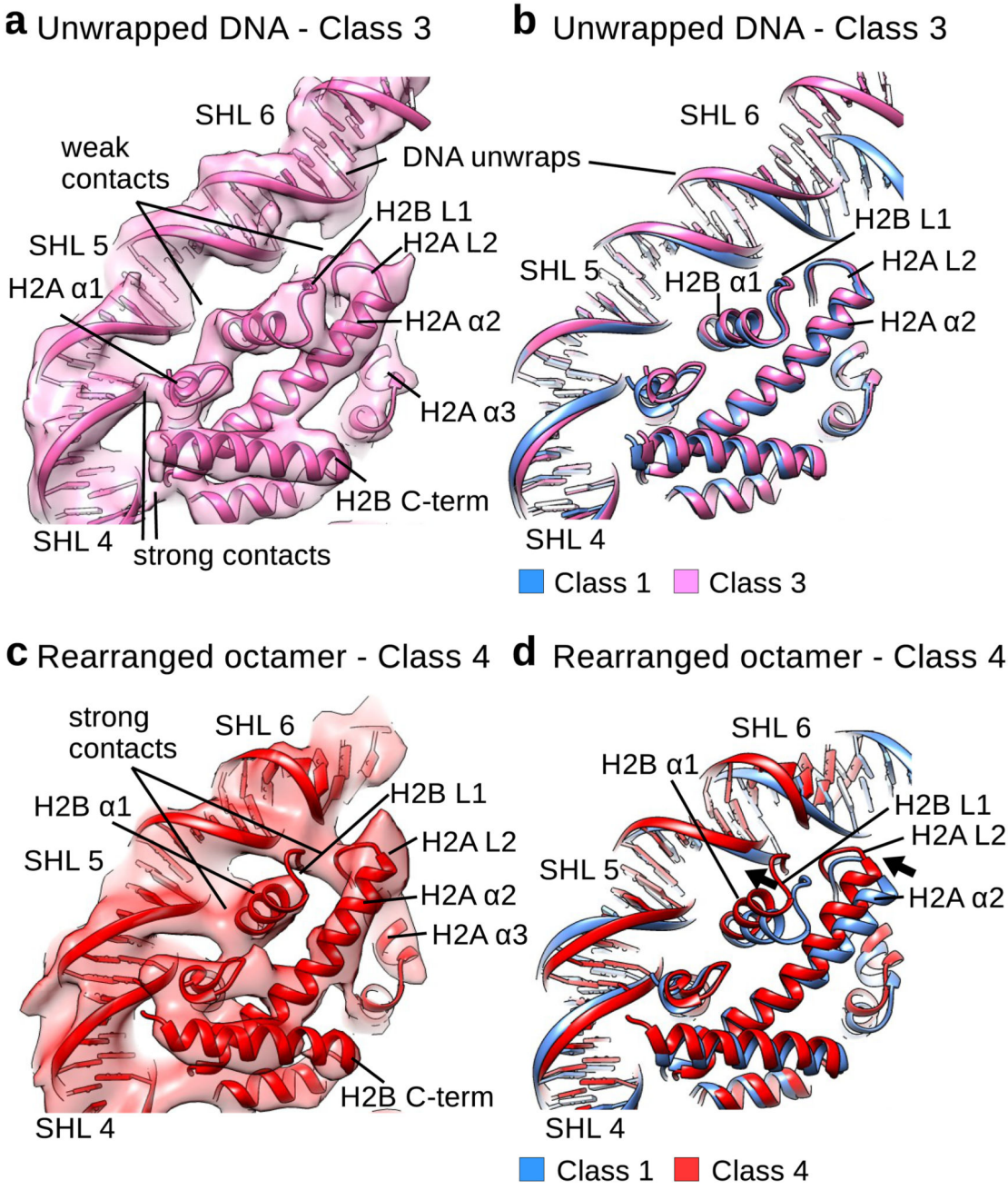

Fig. 3. H2A–H2B dimer rearranges and binds unwrapping DNA.

a, Fitting of the Class 3 model into the cryo EM map. In the Class 3 cryo EM map H2B α1 (SHL 4.5), H2B L1 (H2B α1 and α2) and H2A L2 (H2A α2 and α3) (SHL 5.5) form weaker contacts with the DNA that are only visible at low contour level. H2A α1 at SHL 4.5 and H2A–H2B contacts at SHL 3.5 are similar to the contacts on the side with wrapped DNA.

Europe PMC Funders Author Manuscripts

b, Comparison of the Class 1 model (blue) with the model for the Class 3 (pink) cryo EM map. In the Class 3 structure, H2A–H2B is in the conformation observed in the crystal structure. DNA at SHL 5 moves outward when compared to the Class 1 model.
c, Fitting of the Class 4 model into the cryo EM map. In the Class 4 cryo EM map H2B α1 (SHL 4.5), H2B L1 (H2B α1 and α2) and H2A L2 (H2A α2 and α3) (SHL 5.5) form strong contacts with the DNA that are comparable to other contacts between histones and DNA.
d, Comparison of the Class 1 model (blue) with the model for the Class 4 (red) cryo EM maps. In the Class 4 structure, H2B α1 and α2 and H2A α2 and α3 tilt toward the unwrapping DNA to stabilize the interaction.

Europe PMC Funders Author Manuscripts

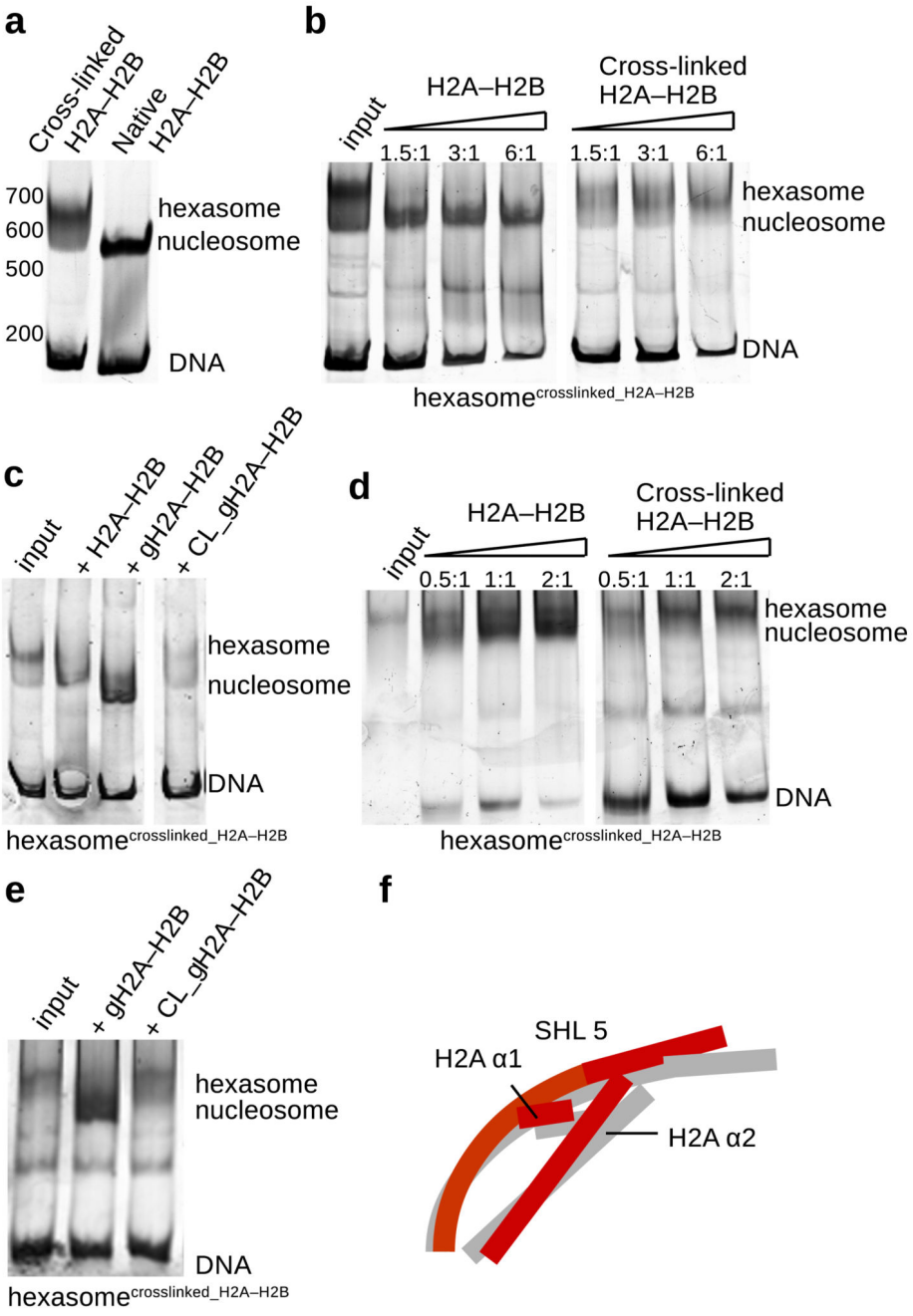

Fig. 4. Cross-linked H2A–H2B is not stably bound to the nucleosome.

a, Native gel showing nucleosome assembly with native and cross-linked H2A–H2B. When nucleosome were assembled with cross-linked H2A–H2B, primarily hexasomes were obtained.

b, Native and cross-linked H2A–H2B were added to the assembled hexasomes **(a)** containing one cross-linked H2A–H2B. Native H2A–H2B is incorporated into hexasome forming the nucleosome. Cross-linked H2A–H2B is not stably incorporated into the hexasome.

c, Native gel showing nucleosome assembly with native and cross-linked globular H2A–H2B. Native and cross-linked globular H2A–H2B were added to the previously assembled hexasomes containing one cross-linked H2A–H2B. Native full length and globular H2A–H2B are incorporated into hexasome forming the nucleosome. Cross-linked globular H2A–H2B is not stably incorporated into the hexasome.

d, Native gel showing Nap1-mediated nucleosome assembly with native and cross-linked H2A–H2B. When we used cross-linked H2A–H2B, Nap1 also primarily assembled hexasomes (input). Native and cross-linked H2A–H2B were added to the assembled hexasomes. Nap1 incorporated native H2A–H2B into hexasomes forming nucleosomes. Nap1 was unable to incorporate cross-linked H2A–H2B into the hexasomes.

e, Native gel showing Nap1-mediated nucleosome assembly with native and cross-linked globular H2A–H2B. Native and cross-linked globular H2A–H2B were added to the assembled hexasomes. Nap1 incorporated native globular H2A–H2B into hexasomes forming nucleosomes. Nap1 was unable to stably incorporate cross-linked globular H2A–H2B into the hexasomes.

f, Unwrapping of DNA at SHL 5.5 induces conformational changes in H2A–H2B. Rearrangement of H2A α2 and α3 and H2B α1 maintains the interaction with the DNA and stabilizes the nucleosome.

Representative images of at least 3 independent experiments are shown. Uncropped gel images are shown in Supplementary Data Set 1.

Europe PMC Funders Author Manuscripts

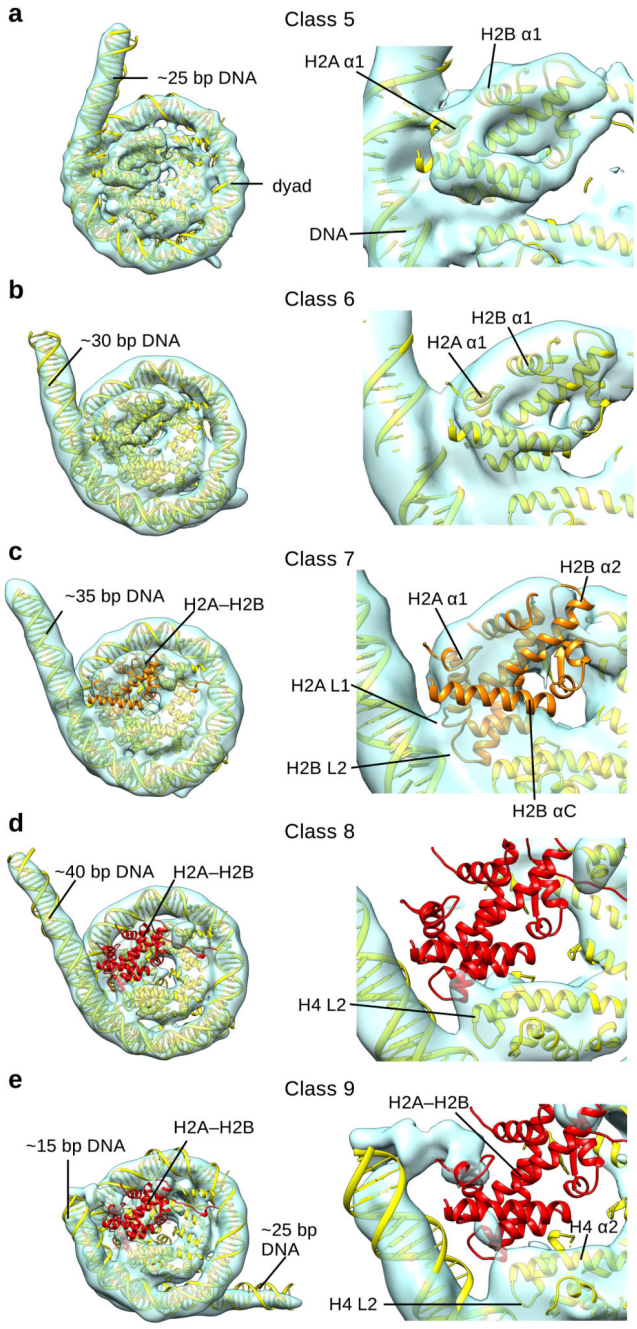

Fig. 5. Cryo-EM reconstructions of distinct NCP and hexasome conformations.

a, Cryo-EM map of NCP (Class 5) with docked model (left). ~25 bp of DNA is not organized by the nucleosome in Class 5. A close view of the H2A–H2B dimer and the last contact with the DNA is shown on the right.

b, Cryo-EM map of NCP (Class 6) with docked model (left). ~30 bp of DNA is not organized by the nucleosome in Class 6. A close view of the H2A–H2B dimer and the last contact with the DNA is shown on the right.

c, Cryo-EM map of NCP (Class 7) with docked model (left). ~35 bp of DNA is not organized by the nucleosome in Class 7. A close view of the H2A–H2B dimer and last contact with the DNA is shown on the right. Only partial density could be observed for the H2A–H2B dimer, colored orange.

d, Cryo-EM map of the hexasome (Class 8) with docked model (left). ~40 bp of DNA is not organized by the nucleosome in Class 8. A close view of the last contact with the DNA is shown on the right. No density for H2A–H2B dimer, colored red, could be observed in the map.

e, Cryo-EM map of the hexasome (Class 9) with docked model (left). ~15 + ~25 bp of DNA is not organized by the nucleosome in Class 9. A close view of the last contact with the DNA is shown on the right. No density for the H2A–H2B dimer, colored red, could be observed in the map.

Europe PMC Funders Author Manuscripts

Table 1
Cryo-EM data collection, refinement, and validation statistics

	Class 1 EMD-3947 PDB ID 6ESF	Class 2 EMD-3948 PDB ID 6ESG	Class 3 EMD-3949 PDB ID 6ESH	Class 4 EMD-3950 PDB ID 6ESI
Data collection and processing				
Magnification	105 000	75 000 / 105 000	75 000 / 105 000	75 000 / 105 000
Voltage (kV)	300	300	300	300
Electron exposure (e–/Å^2)	80	100 / 80	100 / 80	100 / 80
Defocus range (μm)	-1.0 – -4.0	-1.0 – -4.0	-1.0 – -4.0	-1.0 – -4.0
Pixel size (Å)	1.36	1.4 /1.36 (interpolated to 1.4)	1.4 /1.36 (interpolated to 1.4)	1.4 /1.36 (interpolated to 1.4)
Symmetry imposed	C2	C1	C1	C1
Initial particle images (no.)	~ 100 000	~ 700 000	~ 700 000	~ 700 000
Final particle images (no.)	55 000	14 000	22 000	28 000
Map resolution (Å)	3.7	5.1	5.4	6.3
FSC threshold				
Map resolution range (Å)	3.5-4.0	5.0 – 6.0	5.0 – 6.5	6.0 – 7.5
Refinement				
Initial model used	3LZ1	3LZ1	3LZ1	3LZ1
Model resolution (Å)	3.7	5.1	5.4	6.3
FSC threshold				
Model resolution range (Å)	228-3.7	235-5.1	235-5.4	235-6.3
Map sharpening *B* factor (Å^2)	-150	-150	-200	-100
Model composition				
Nonhydrogen atoms	12091	11515	11474	11173
Protein residues	762	725	738	719
Ligand				
B factors (Å^2)				
Protein	74.74	227.3	256.47	388.20
Ligand				
R.m.s. deviations				
Bond lengths (Å)	0.008	0.007	0.007	0.008
Bond angles (°)	0.961	0.957	1.091	1.084

	Class 1 EMD-3947 PDB ID 6ESF	Class 2 EMD-3948 PDB ID 6ESG	Class 3 EMD-3949 PDB ID 6ESH	Class 4 EMD-3950 PDB ID 6ESI
Validation				
MolProbity score	1.62	1.92	1.71	2.11
Clashscore	5.52	10.87	7.34	15.86
Poor rotamers (%)	0.94	0.50	0.65	0.83
Ramachandran plot				
Favored (%)	95.58	96.05	96.13	93.99
Allowed (%)	4.42	3.95	3.87	5.87
Disallowed (%)	0.00	0.00	0.00	0.14

Europe PMC Funders Author Manuscripts

Europe PMC Funders Author Manuscripts

Table 2

Cryo-EM data collection, refinement, and validation statistics

	Class 5 (EMD-3931)	Class 6 (EMD-3930)	Class 7 (EMD-3929)	Class 8 (EMD-3926)	Class 9 (EMD-3925)
Data collection and processing					
Magnification	75 000	75 000	75 000	75 000	75 000
Voltage (kV)	300	300	300	300	300
Electron exposure (e–/Å^2)	100	100	100	100	100
Defocus range (μm)	-1.0 – -4.0	-1.0 – -4.0	-1.0 – -4.0	-1.0 – -4.0	-1.0 – -4.0
Pixel size (Å)	1.4	1.4	1.4	1.4	1.4
Symmetry imposed	C1	C1	C1	C1	C1
Initial particle images (no.)	~100 000	~100 000	~100 000	~100 000	~100 000
Final particle images (no.)	25 000	14 000	14 000	16 000	9 000
Map resolution (Å) FSC threshold	8.0	10.5	10.5	10.5	8.5
Map resolution range (Å)	8.0 - 15	9.0 - 15	9.0 - 15	10.0 - 15	9.0 - 15